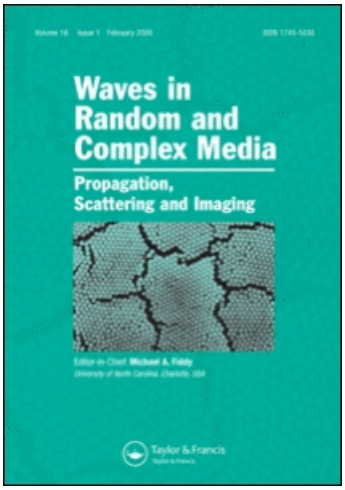

Waves in Random and Complex Media
Publication details, including instructions for authors and subscription information:
http://www.informaworld.com/smpp/title~content=t716100762

A monostatic illumination function with surface reflections from one-dimensional rough surfaces

Hongkun Li[a]; Nicolas Pinel[a]; Christophe Bourlier[a]
[a] Université de Nantes—IREENA Laboratory, Ecole Polytechnique de L'Université de Nantes, 44306 Nantes Cedex 3, France

Online publication date: 28 January 2011

To cite this Article Li, Hongkun , Pinel, Nicolas and Bourlier, Christophe(2011) 'A monostatic illumination function with surface reflections from one-dimensional rough surfaces', Waves in Random and Complex Media, 21: 1, 105 — 134
To link to this Article: DOI: 10.1080/17455030.2010.524263
URL: http://dx.doi.org/10.1080/17455030.2010.524263

Waves in Random and Complex Media
Vol. 21, No. 1, February 2011, 105–134

Taylor & Francis
Taylor & Francis Group

A monostatic illumination function with surface reflections from one-dimensional rough surfaces

Hongkun Li*, Nicolas Pinel and Christophe Bourlier

Université de Nantes—IREENA Laboratory, Ecole Polytechnique de L'Université de Nantes, Rue Christian Pauc, La Chantrerie, BP 50609, 44306 Nantes Cedex 3, France

(*Received 5 March 2010; final version received 7 September 2010*)

When solving scattering or emissivity problems for rough surfaces, the shadowing effect is often taken into account. Furthermore, for rough surfaces with large root mean square slope, surface reflections of the incidence or emission ray should not be neglected, especially at large observation angles. In this paper, a model of the monostatic statistical illumination function for one-dimensional rough surfaces with single surface reflection is developed, which is based on the Smith illumination function. A Monte Carlo ray-tracing algorithm is used to evaluate the accuracy of the present model. It is shown that, when neglecting the correlation between heights and slopes of the surface, the present model agrees quite well with the Monte Carlo result. Moreover, the result is improved if the correlation between heights and slopes is taken into account. For practical purposes, an empirical factor is introduced to improve the performance of the uncorrelated first-order illumination function to avoid computing the correlated one, which takes a long computation time. Besides, the first-order illumination function is significant at large observation angles, which could be promising to overcome problems in models of surface infrared emissivity where underestimation occurs compared with experimental measurements.

1. Introduction

Shadowing is an important aspect in solving scattering and emissivity related problems of rough surfaces. Conventional illumination functions, for example Wagner's model [1] and Smith's model [2], can be dated back to the 1960s, and are widely used in models of scattering and emissivity. In these early models, correlation between heights and slopes of the surface is neglected. Bourlier et al. [3] compared the Wagner, Smith and Ricciardi–Sato models [4,5], and concluded that Smith's illumination function is the most accurate and that considering the correlation only weakly improves the result. Besides, he extended Smith's model by introducing the length of the surface to obtain the illumination function of a surface with finite length.

*Corresponding author. Email: hongkun.li@etu.univ-nantes.fr

ISSN 1745–5030 print/ISSN 1745–5049 online

DOI: 10.1080/17455030.2010.524263
http://www.informaworld.com

Moreover, the higher accuracy requirement in solving infrared emissivity problems of rough surfaces demands that surface reflections should be taken into account, as the surface infrared emissivity is underestimated when compared with experimental measurements at large observation angles [6–8]. Illumination with surface reflections is considered in some models. Wu and Smith [6] defined a cutoff angle (measured from the zenith), which is compared with the reflection angles. For those reflection angles smaller than the cutoff angle, surface reflection was assumed to be negligible, while for those larger than the cutoff angle, the illumination function with surface reflections was given empirically. As Wu and Smith admitted themselves, it was hard to define the cutoff angle because of lack of knowledge. Masuda [8] defined a weighting function to avoid defining an exact cutoff angle. However, he described his illumination factor as a normalization factor instead of a statistical expression. Bourlier et al. [9] developed a statistical illumination function with surface reflections; however, his model underestimated the illumination effect to a large extent.

To meet the higher accuracy requirement, a more precise model of the statistical illumination function with surface reflection is developed in this paper. To avoid too much complexity, a one-dimensional surface with infinite length is considered under a monostatic configuration, as there exists only a receiver. The surface is modeled as being single-valued, and the geometric optics approximation (GO) is assumed to be valid, which describes the rough surface as a series of continuous smooth facets which reflect rays specularly.

This model was originally designed for infrared wavelengths, especially for solving sea surface infrared emissivity. As the geometric optics approximation (GO) is employed, the studied wavelength must be much smaller than the surface curvature radius [10]. In other words, the surface should be locally smooth under the studied wavelength. When studying the infrared emissivity of a sea surface, this condition is fulfilled even if capillary waves are present, as the studied electromagnetic wavelength is of the order of about 10 μm while the wavelength of a capillary wave is of the order of 1 cm. This model can be applied to other wavelengths, on condition that the surface is smooth enough and that GO is valid.

Section 2 summarizes the Smith illumination function, in which no surface reflection is considered.

In Section 3, the illumination function with single surface reflection is derived. Four geometric configurations of single surface reflection are investigated, and the illumination function for each configuration, without considering the correlation between heights and slopes, is given.

In Section 4, the present model is compared with the result of a Monte Carlo algorithm, which is based on ray-tracing. It is shown that the uncorrelated illumination function, with and without surface reflections, agrees quite well with the Monte Carlo method, but overestimates the illumination effect at large observation angles. The contribution of correlation between heights and slopes is studied in detail, and it is proved that considering the correlation improves the result. A short discussion on the illumination effect and the surface reflection effect is given.

Section 5 introduces an empirical factor to improve the performance of the zero-order and first-order uncorrelated illumination functions. After correcting by

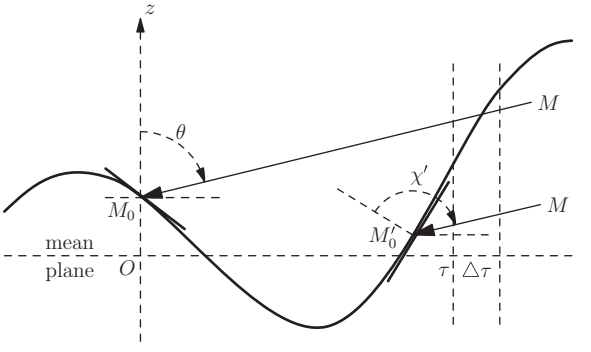

Figure 1. Illumination without reflection.

the empirical factor, the uncorrelated illumination function is able to match the performance of the correlated one.

Section 6 gives concluding remarks.

2. Statistical illumination function without reflection

2.1. *Formulation without correlation*

The monostatic statistical illumination function without reflection is related to the probability that an arbitrary point of the rough surface does not lie in shadow when the surface is illuminated by an incident ray along an observation angle θ. As Bourlier et al. [3] showed that Smith's model [2] is the most accurate one, in this paper, we adopt Smith's model as the basic model. Smith developed this probability by introducing a ray emitted from an arbitrary point M_0 on the surface, with height ζ_0 and slope γ_0, along the observation angle, as shown in Figure 1. The surface is assumed to be single-valued, and the sensor M is put at the right-hand side of the surface at an infinite distance. As a result, $\theta > 0$ (θ is measured clockwise from zenith). Smith studied the probability that this ray does not cross the surface, which is equal to the probability that M_0 is illuminated by the incident ray.

The derivation of the Smith illumination function is shown in Appendix 1, and the result is expressed as [2]:

$$S(\mu, \gamma_0, \zeta_0, L_0) = A \cdot \exp\left[- \int_0^{L_0} g(\mu|\gamma_0, \zeta_0; \tau) \mathrm{d}\tau \right], \tag{1}$$

where $\mu = \cot\,\theta$ is the slope of the incident ray, and L_0 is the surface length introduced by Bourlier et al. [3]. The function $g(\mu|\gamma_0, \zeta_0; \tau)$ is given by:[1]

$$g(\mu|\gamma_0, \zeta_0; \tau) = \frac{\displaystyle\int_{\mu}^{+\infty} (\gamma - \mu)\, p(\zeta = \zeta_0 + \mu\tau, \gamma|\zeta_0, \gamma_0; \tau) \mathrm{d}\gamma}{\displaystyle\int_{-\infty}^{+\infty} \int_{-\infty}^{\zeta_0 + \mu\tau} p(\zeta, \gamma|\zeta_0, \gamma_0; \tau) \mathrm{d}\gamma \mathrm{d}\zeta}. \tag{2}$$

The factor A can be an arbitrary constant. However, the choice of A affects the physical solution heavily, especially when this model is extended to deal with surface reflections, which is the aim of the next section. First of all, $S(\mu, \gamma_0, \zeta_0, L_0)$ should be unity when $\theta = 0$, because no shadow is produced by such a vertically incident ray, as the surface is assumed to be single-valued. Secondly, as M_0 is chosen randomly, it is obvious that the slope of M_0 must obey $\gamma_0 < \mu$, otherwise the local incidence angle χ' exceeds 90° and the introduced ray would go inside the surface (see the ray $\boldsymbol{M_0'M}$ in Figure 1), in which case M_0 lies in shadow and the deduction is neither valid nor necessary. As a result, Smith chose A as the Heaviside function:

$$A = \Upsilon(\mu - \gamma_0) = \begin{cases} 0, & \gamma_0 > \mu \\ 1, & \gamma_0 < \mu. \end{cases} \tag{3}$$

The problem of simplifying Equation (1) is that the conditional probability density function (PDF) $p(\zeta, \gamma|\zeta_0, \gamma_0; \tau)$ is of great complexity. The calculation considering such a correlation is fully developed by Bourlier et al. and is reviewed briefly in Appendix 2. Neglecting the correlation between heights and slopes provides great simplicity in calculation. Substituting Equations (2) and (3) into Equation (1), while neglecting the correlation, the integration over τ leads to [3]:

$$S(\mu, \gamma_0, \zeta_0, L_0) = \Upsilon(\mu - \gamma_0) \times \left[\frac{F(\zeta_0) - F(-\infty)}{F(\zeta_0 + \mu L_0) - F(-\infty)}\right]^{\Lambda(\mu)}, \tag{4}$$

while for a surface with infinite length $L_0 \to \infty$, it is simplified as:

$$S(\mu, \gamma_0, \zeta_0) = \Upsilon(\mu - \gamma_0) F(\zeta_0)^{\Lambda(\mu)}, \tag{5}$$

with $F(\zeta)$ the cumulative density function (CDF) of the height PDF $p_\zeta(\zeta)$:

$$F(\zeta_0) = \int_{-\infty}^{\zeta_0} p_\zeta(\zeta) \mathrm{d}\zeta, \tag{6}$$

and

$$\Lambda(\mu) = \frac{1}{\mu} \int_{\mu}^{+\infty} (\gamma - \mu)\, p_\gamma(\gamma) \mathrm{d}\gamma, \tag{7}$$

where $p_\gamma(\gamma)$ is the slope PDF.

Equation (4) or (5) is called the statistical zero-order illumination function, denoted as S_0, whose subscript indicates the number of reflections. Equations (4) and (5) both consist of two terms: the first term is the Heaviside function, which involves the slope of the point M_0; the second term involves the cumulative density function (CDF) of the height of the point M_0. The first term restricts the slope of the illuminated facets to a region where the local incidence angle does not exceed 90°, while the second term computes the probability that the ray $M_0(\theta)$ is blocked during propagation.

2.2. *Case of a Gaussian PDF*

For a given slope PDF, the statistical zero-order illumination function can be averaged over the whole surface and thus expresses the proportion of the illuminated part over the whole surface. For a surface of infinite length, the average zero-order illumination function is given by averaging Equation (5) over the height ζ_0 and the slope γ_0 of M_0:

$$\overline{\overline{S}}_0(\mu) = \int_{-\infty}^{+\infty}\int_{-\infty}^{+\infty} \Upsilon(\mu-\gamma_0)F(\zeta_0)^{\Lambda(\mu)} p_\zeta(\zeta_0)\, p_\gamma(\gamma_0)\mathrm{d}\zeta_0\mathrm{d}\gamma_0. \tag{8}$$

The integration of the zero-order illumination function over the height ζ_0 results in:

$$\overline{S}_0(\mu,\gamma) = \frac{\Upsilon(\mu-\gamma_0)}{1+\Lambda(\mu)}. \tag{9}$$

Equation (9) holds for any height PDF. However, the integration over the slope γ_0 requires knowledge of the slope PDF. For computational ease, the surface slope PDF is assumed to be Gaussian here, with zero mean and RMS slope σ_γ:

$$p_\gamma(\gamma) = \frac{1}{\sigma_\gamma\sqrt{2\pi}}\exp\left(-\frac{\gamma^2}{2\sigma_\gamma^2}\right). \tag{10}$$

The average zero-order illumination function is then obtained:

$$\overline{\overline{S}}_0(v) = \frac{1}{1+\Lambda(v)}\left[1-\frac{1}{2}\mathrm{erfc}(v)\right], \tag{11}$$

with erfc the complementary error function, and

$$\begin{cases} \Lambda(v) = \dfrac{\exp(-v^2) - v\sqrt{\pi}\mathrm{erfc}(v)}{2v\sqrt{\pi}} \\ v = \dfrac{\mu}{\sqrt{2}\sigma_\gamma} \quad \mu = \cot\theta. \end{cases} \tag{12}$$

Bourlier et al. [3] compared Equation (11) with the result of a Monte Carlo ray-tracing algorithm. He concluded that Equation (11) slightly overestimates the illumination effect.

However, as indicated by references [6–8], to calculate emissivity with accuracy, higher order surface reflections must be taken into account for higher accuracy. In the following section, the illumination function with single surface reflection is developed in a statistical way.

3. Statistical illumination function with one surface reflection

The statistical first-order illumination function (with one surface reflection) gives the probability that an arbitrary point M_1 of the surface is illuminated by the sensor M

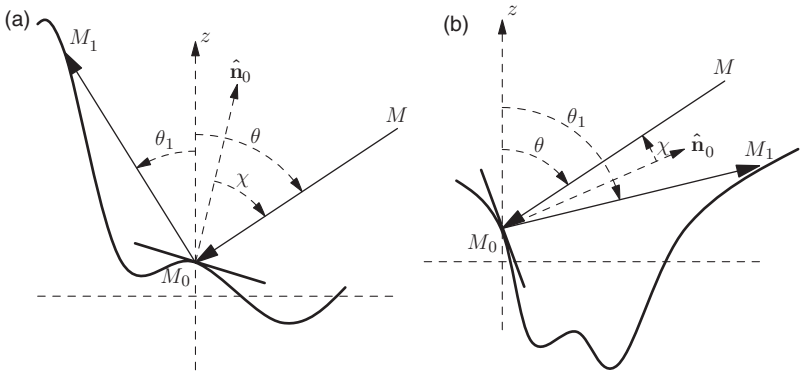

Figure 2. Reflection occurs at point M_0 when $\theta_1 < 0$ (a) and $\theta_1 > 0$ (b).

after the incident ray is reflected by some other point M_0 on the surface. Figure 2 illustrates such reflections for two cases.

3.1. *Determination of the problem under approximations*

The problem can be expressed equally as determining the probability that the ray $\boldsymbol{M_0M}$ of angle θ (denoted as $M_0(\theta)$) does not cross the surface, while the ray $\boldsymbol{M_0M_1}$ of angle θ_1 (denoted as $M_0(\theta_1)$) crosses the surface, which can be written mathematically as:

$$\begin{aligned} S_1 &= p(M_0(\theta) \text{ does not cross } \cap M_0(\theta_1) \text{ crosses}) \\ &= p(M_0(\theta) \text{ does not cross}) \\ &\quad \times p(M_0(\theta_1) \text{ crosses} \mid M_0(\theta) \text{ does not cross}) \\ &= p(M_0(\theta) \text{ does not cross}) \\ &\quad \times [1 - p(M_0(\theta_1) \text{ does not cross} \mid M_0(\theta) \text{ does not cross})] \\ &= p(a)[1 - p(b|a)] \end{aligned}$$

with '$M_0(\theta)$ does not cross the surface' denoted symbolically as 'a' and '$M_0(\theta_1)$ does not cross the surface' as 'b'. The probability $p(a)$ corresponds to the statistical zero-order illumination function given by Equation (1), while $p(b)$ is obtained similarly by:

$$p(b) = A \cdot \exp\left[- \int_{\tau_{\min}}^{\tau_{\max}} g(\mu_1 | \gamma_0, \zeta_0; \tau) \mathrm{d}\tau \right], \tag{13}$$

where $\tau \in [\tau_{\min}, \tau_{\max}]$ indicates the integration range of τ: $\tau \in (-\infty, 0]$ for $M_0(\theta)$ going leftward, whereas $\tau \in [0, +\infty)$ for $M_0(\theta)$ going rightward.

There is a strong correlation between events a and b. The event '$M_0(\theta)$ *does not cross the surface*' is the prerequisite for the existence of $M_0(\theta_1)$: $M_0(\theta_1)$ is the reflected

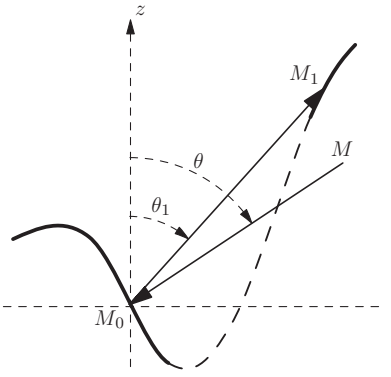

Figure 3. The $0<\theta_1<\theta$ situation.

ray of $M_0(\theta)$. It makes θ_1 different from θ: θ_1 is the reflection angle which depends on θ and on the slope of M_0, whereas θ is an arbitrary angle ranging from 0 to $\pi/2$ (assuming that the sensor is at the right-hand side of the surface). The constant A for $p(b)$ must check that $M_0(\theta_1)$ does not go into the surface at the very beginning. For example, for $\theta_1<0$ (Figure 2(a)), A must equal $\Upsilon(\gamma_0-\mu_1)$, with μ_1 the slope of the reflection ray. However, knowing that $M_0(\theta)$ does not cross the surface gives information on both the slope of M_0 and $M_0(\theta_1)$. As $M_0(\theta_1)$ is the reflected ray of $M_0(\theta)$, it is obvious that $\gamma_0>\mu_1$ is satisfied, which means that A must be set to $A\equiv 1$. In another situation shown in Figure 2(b) where $\theta_1>0$, A for $p(b)$ must equal $\Upsilon(\mu_1-\gamma_0)$. Knowing that $M_0(\theta)$ does not cross the surface leads to the same result that $\mu_1>\gamma_0$ is always satisfied, thus $A\equiv 1$. The reason can be explained physically as: a reflected ray never goes into the surface. As a result, $p(b|a)$ is obtained approximately by modifying $p(b)$ as:

$$p(b|a)\approx\exp\left[-\int_{\tau_{\min}}^{\tau_{\max}} g(\mu_1|\gamma_0,\zeta_0;\tau)\mathrm{d}\tau\right],\quad \text{for } p(a)\neq 0. \tag{14}$$

Besides, the event '$M_0(\theta)$ *does not cross the surface*' restricts the range of θ_1. Figure 3 illustrates the situation in which $0<\theta_1<\theta$. As the surface is assumed to be single-valued and as the sensor is assumed to be infinitely far from any surface point, some point between M_1 and M_0 would surely block M_0 from the sensor, which conflicts with the assertion '$M_0(\theta)$ *does not cross the surface*'. In such a case, the event a cannot happen. As a result, we set

$$S_1=0,\quad \text{for } 0<\theta_1<\theta \Leftrightarrow p(a)=0. \tag{15}$$

The first-order statistical illumination function is then derived:

$$S_1(\mu,\gamma_0,\zeta_0)=\begin{cases}0, & 0<\theta_1<\theta\\ S_0(\mu,\gamma_0,\zeta_0)\left\{1-\exp\left[\displaystyle\int_{\tau_{\min}}^{\tau_{\max}} g(\mu_1|\gamma_0,\zeta_0;\tau)\mathrm{d}\tau\right]\right\}, & \text{otherwise.}\end{cases} \tag{16}$$

3.2. *Geometric calculation of the reflection*

Equation (16) involves the slope μ_1 of the reflected ray. In this subsection, we calculate the reflection angle θ_1, from which $\mu_1 = \cot\theta_1$ is derived.

The vector $\hat{\boldsymbol{n}}_0$ is the unitary normal vector of the facet at point M_0 (see Figure 2). It is given by

$$\hat{\boldsymbol{n}}_0 = (-\gamma_0,\ 1)/(1+\gamma_0^2)^{1/2}. \tag{17}$$

We denote $\hat{\boldsymbol{m}}_0 = (\sin\theta, \cos\theta)$ as the unitary vector of the ray $\boldsymbol{M_0M}$. Thus, the local incidence angle χ_0 is given by

$$\cos\chi_0 = \hat{\boldsymbol{n}}_0 \cdot \hat{\boldsymbol{m}}_0 = \frac{\cos\theta - \gamma_0\sin\theta}{(1+\gamma_0^2)^{1/2}}. \tag{18}$$

With knowledge of θ and γ_0, the unitary vector $\hat{\boldsymbol{m}}_1 = (\sin\theta_1, \cos\theta_1)$ of the reflected ray $\boldsymbol{M_0M_1}$ can be calculated as:

$$\hat{\boldsymbol{m}}_1 = 2(\hat{\boldsymbol{n}}_0 \cdot \hat{\boldsymbol{m}}_0)\hat{\boldsymbol{n}}_0 - \hat{\boldsymbol{m}}_0 = 2\cos\chi_0\hat{\boldsymbol{n}}_0 - \hat{\boldsymbol{m}}_0.$$

Thus, the reflection angle is given by:

$$\begin{aligned}\cos\theta_1 = \hat{\boldsymbol{m}}_1 \cdot \hat{\boldsymbol{z}} &= 2\frac{\cos\theta - \gamma_0\sin\theta}{1+\gamma_0^2} - \cos\theta \\ &= \cos\theta\left[2g_0(1+\gamma_0^2)^{-1} - 1\right],\end{aligned} \tag{19}$$

where

$$g_0 = 1 - \gamma_0\tan\theta. \tag{20}$$

Equation (19) gives the cosine of θ_1. However, to obtain θ_1 or $\cot\theta_1$, the sign of θ_1 must be calculated. Recalling that an angle is positive if measured clockwise from the zenith, the sign of θ_1, denoted as t_1, is calculated by:[2]

$$\begin{cases} t_1 = +1, & \gamma_0 < -\tan(\theta/2) \\ t_1 = -1, & \gamma_0 > -\tan(\theta/2). \end{cases}$$

The oriented θ_1 is then expressed by:

$$\theta_1 = t_1 \cdot \arccos\left\{\cos\theta\left[2g_0(1+\gamma_0^2)^{-1} - 1\right]\right\}, \tag{21}$$

and the slope of the reflection ray μ_1 is obtained by $\mu_1 = \cot\theta_1$.

3.3. *Simplification without correlation under four configurations*

Figure 4 illustrates the four configurations in which surface reflections happen. In cases 1 and 2, $\theta_1 > 0$, which corresponds to Figure 2(b). In cases 3 and 4, $\theta_1 < 0$, which corresponds to Figure 2(a). In case 2, restriction should be put to θ_1 according to Equation (15). Equation (16) can be greatly simplified according to each configuration.

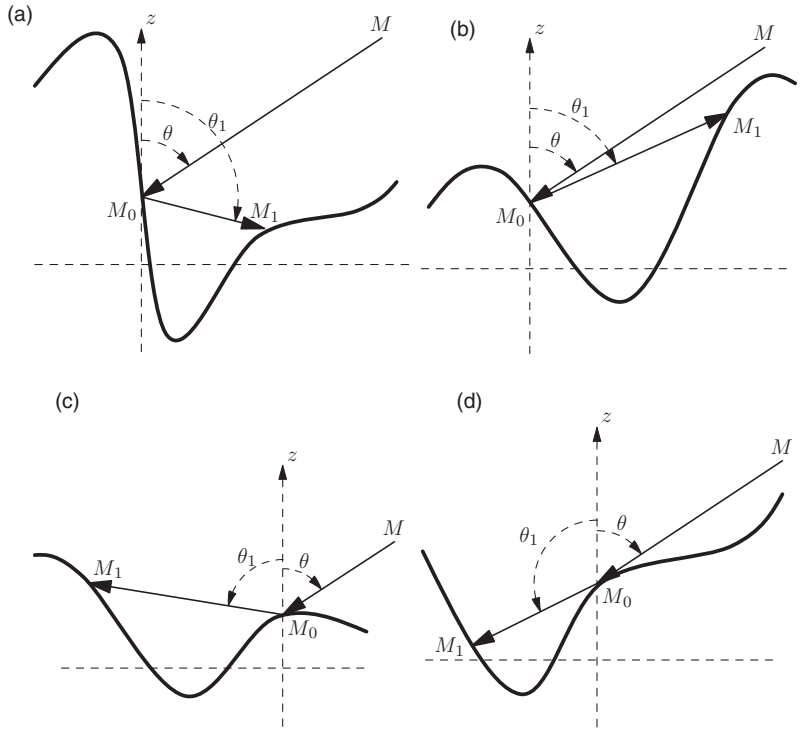

Figure 4. The four configurations of surface reflection. (a) Case 1, where $\pi/2<\theta_1<\pi$; (b) case 2, where $\theta<\theta_1<\pi/2$; (c) case 3, where $-\pi/2<\theta_1<0$; (d) case 4, where $-\pi<\theta_1<-\pi/2$.

To clearly distinguish these four configurations, another parameter $q_1=$ sign$(\cos\theta_1)$ is introduced, which indicates whether M_1 is higher or lower than M_0:

$$\begin{cases} q_1=+1, & 0<|\theta_1|<\pi/2 \quad \Leftrightarrow \quad M_1 \text{ higher than } M_0 \\ q_1=-1, & \pi/2<|\theta_1|<\pi \quad \Leftrightarrow \quad M_1 \text{ lower than } M_0. \end{cases}$$

Accordingly, these four cases can be identified by t_1 and q_1 as:

$$\begin{cases} \text{case 1} & \{q_1=-1, t_1=+1\} & \Leftrightarrow & \pi/2<\theta_1<\pi \\ \text{case 2} & \{q_1=+1, t_1=+1, \theta_1>\theta\} & \Leftrightarrow & \theta<\theta_1<\pi/2 \\ \text{case 3} & \{q_1=+1, t_1=-1\} & \Leftrightarrow & -\pi/2<\theta_1<0 \\ \text{case 4} & \{q_1=-1, t_1=-1\} & \Leftrightarrow & -\pi<\theta_1<-\pi/2. \end{cases}$$

As θ_1 is a function of θ and γ_0 (see Equation (21)), these four cases can also be identified by γ_0. In Appendix 3, four threshold values of γ_0 are calculated, according

to which four cases are defined:

$$\begin{cases} \text{case 1} & -\infty < \gamma_0 < -\tan(\pi/4+\theta/2) \\ \text{case 2} & -\tan(\pi/4+\theta/2) < \gamma_0 < -\tan(\theta) \\ \text{case 3} & -\tan(\theta/2) < \gamma_0 < \tan(\pi/4-\theta/2) \\ \text{case 4} & \tan(\pi/4-\theta/2) < \gamma_0 < \cot(\theta). \end{cases} \tag{22}$$

The correlation between heights and slopes is neglected here. For cases 1 and 4, $p(b|a)=0$. This can be calculated strictly as shown in Appendix 4, or more physically, it can be explained as: a ray heading downward certainly crosses the surface. For cases 2 and 3, the result is given as:[3]

$$p(b|a) = F(\zeta_0)^{\Lambda(\mu_1)}. \tag{23}$$

Finally, the statistical first-order illumination function is obtained:

$$S_1(\mu,\gamma_0,\zeta_0) = \begin{cases} F(\zeta_0)^{\Lambda(\mu)}, & \text{cases 1\&4} \\ F(\zeta_0)^{\Lambda(\mu)}\left[1-F(\zeta_0)^{\Lambda(\mu_1)}\right], & \text{cases 2\&3} \\ 0, & \text{otherwise,} \end{cases} \tag{24}$$

where $\Lambda(\mu)$ is given by Equation (7) and

$$\begin{cases} \Lambda(\mu_1) = \dfrac{1}{\mu_1}\displaystyle\int_{\mu_1}^{+\infty}(\gamma-\mu_1)\,p_\gamma(\gamma)\mathrm{d}\gamma, & \text{for } \theta_1 > 0 \\ \Lambda(\mu_1) = \dfrac{1}{\mu_1}\displaystyle\int_{-\infty}^{\mu_1}(\gamma-\mu_1)\,p_\gamma(\gamma)\mathrm{d}\gamma, & \text{for } \theta_1 < 0. \end{cases} \tag{25}$$

Recall that the zero-order illumination function involves the slope of the facet γ_0 by the Heaviside function $\Upsilon(\mu-\gamma_0)$, which gives two alternatives only: the facet is either possible ($\Upsilon=1$) or impossible ($\Upsilon=0$) to illuminate. However, the first-order illumination function is more complicated, as it involves an incident ray and the reflected ray. It involves the slope of the facet γ_0 by dividing the range of γ_0 into five ranges (four cases and otherwise), where three possibilities (see Equation (24)) are found accordingly. In the range where γ_0 belongs to cases 1 and 4, the reflected ray goes downward, which surely intersects the surface. Thus, the first-order illumination function requires only the calculation of the probability that the point M_0 is viewed by the sensor, which equals exactly $F(\zeta_0)^{\Lambda(\mu)}$. In the range where γ_0 belongs to cases 2 and 3, the reflected ray goes upward. Thus, the first-order illumination function requires considering additionally the probability that the reflected ray $M_0(\theta_1)$ crosses the surface during propagation. As a result, the first-order illumination function in cases 2 and 3 has an additional term $1-F(\zeta_0)^{\Lambda(\mu_1)}$. Beyond the above four cases, γ_0 lies in unphysical ranges, where it is impossible to observe surface reflection.

3.4. *Average first-order illumination function*

To see the performance of the presented model, the average first-order illumination function is studied in this subsection. Integrating Equation (24) over the height and

the slope of M_0 leads to the average first-order illumination function:

$$\overline{\overline{S}}_1(\mu) = \int_{-\infty}^{+\infty} \int_{-\infty}^{+\infty} S_1(\mu, \gamma_0, \zeta_0)\, p_\zeta(\zeta_0)\, p_\gamma(\gamma_0) \mathrm{d}\zeta_0 \mathrm{d}\gamma_0. \tag{26}$$

The integration over ζ_0 can be calculated analytically and it does not depend on the height PDF. The result is shown as follows:

$$\overline{S}_1(v, \gamma_0) = \begin{cases} \dfrac{1}{\Lambda(v)+1}, & \text{cases 1\&4} \\ \dfrac{\Lambda(v_1)}{[\Lambda(v)+1][\Lambda(v_1)+\Lambda(v)+1]}, & \text{cases 2\&3} \\ 0, & \text{otherwise.} \end{cases} \tag{27}$$

where $v = \mu/(\sqrt{2}\sigma_\gamma)$, $v_1 = \mu_1/(\sqrt{2}\sigma_\gamma)$. However, the integration over γ_0 is more difficult to derive, because θ_1 is a function of γ_0. Besides, the surface slope PDF should be known. As a result, it is calculated numerically, with the slope PDF assumed to be Gaussian. The result is shown in the next section.

3.5. *Discussion on the first-order illumination function*

It is noticeable that this statistical first-order illumination function S_1 depends on the incidence angle θ (or equally on the slope of the incident ray $\mu = \cot\theta$), the height and the slope of M_0 and the slope PDF, while surprisingly, the height and the slope of M_1 have no influence on S_1. Bourlier et al. [9] developed a statistical illumination function with multiple surface reflections, where the statistical first-order illumination function[4] is expressed in terms of the slopes and the heights of both M_0 and M_1. The difference comes from the different expression for M_1. In the model developed here, M_1 is an uncertain point, which exists but whose exact position is unknown and of no importance. Bourlier et al. defined the position of M_1 to be the end of an observation length $\tau = l_1$. However, l_1 is in fact the length of the subsurface $\tau \in (0, l_1)$ and $S(\mu, \gamma_0, \zeta_0, l_1)$ only gives the probability that the ray $M_0(\theta)$ crosses this subsurface, which does not ensure that M_1 is at the point $\tau = l_1$. Besides, Bourlier et al. considered only the situations in which the ray $M_0(\theta_1)$ is traveling leftward, while the model here considers both directions. Considering the reflected ray traveling in both directions is very important, especially for surfaces with large RMS slopes. In cases 1 and 2, the reflected ray goes rightward. Note that in these two cases, γ_0 has large values. For a surface with small RMS slopes σ_γ, 0.2 for example, the contribution of cases 1 and 2 is weak. However, as σ_γ increases, to 0.5 for example, the contribution of cases 1 and 2 becomes significant. These results are shown in Figure 7. Bourlier et al. did not compare his first-order illumination function with the Monte Carlo result in reference [9]. However, he developed another similar model [11], which did not overcome the previous two drawbacks, to calculate the surface emissivity. The result shows that his model underestimates the illumination effect greatly.

Although the first-order illumination function does not depend on M_1, it does restrict the height and the slope of M_1. As discussed in Section 3.3, the event

'ray $M_0(\theta_1)$ crosses the surface' does not place a restriction on M_0. However, as $M_0(\theta_1)$ propagates into the facet of M_1, it gives a restriction to the height and the slope of M_1 according to the value of the parameters q_1 and t_1:

$$\begin{cases} \zeta_1 \in (\zeta_0, +\infty) & \text{if } q_1 = +1 \\ \zeta_1 \in (-\infty, \zeta_0) & \text{if } q_1 = -1 \end{cases} \tag{28a}$$

$$\begin{cases} \gamma_1 \in (\mu_1, +\infty) & \text{if } t_1 = +1 \\ \gamma_1 \in (-\infty, \mu_1) & \text{if } t_1 = -1. \end{cases} \tag{28b}$$

The above restrictions should be taken into account when determining some parameters which depend on the height and the slope of M_1 and on this illumination function, for example the surface reflected emissivity.

4. Numerical calculation

In this section, numerical results of the present model, with and without correlation, are shown, compared with the result of the Monte Carlo method.

In the previous parts of this paper, correlation between heights and slopes was neglected, which allows significant simplification of the equations and reduces the computation time. Bourlier et al. [3,11] studied the effect of correlation between heights and slopes of the surface in the zero- and first-order illumination functions and showed that considering correlation improves the accuracy. The calculation of the correlated zero- and first-order illumination function is shown in Appendix 2. The Monte Carlo ray-tracing method is explained in reference [3,11]. In the algorithm, a rough surface is generated, over which an incident ray is put. Every point of the surface is checked and marked whether it is illuminated by the incident ray. For the first-order illumination, the reflected rays are also traced to see whether they cross the surface. In this section, Bourlier's formulations with correlation are used, together with the same Monte Carlo method.

4.1. *Marginal histograms of zero-order illumination function*

Marginal histograms of the illuminated slope and height are useful parameters to evaluate the performance of the corresponding illumination function. The zero-order marginal histograms of illuminated slopes and heights are defined as:

$$\widetilde{p}_{\gamma}^{0}(\mu, \gamma_0) = \int_{-\infty}^{+\infty} S_0(\mu, \gamma_0, \zeta_0)\, p_{\gamma}(\gamma_0)\, p_{\zeta}(\zeta_0) \mathrm{d}\zeta_0, \tag{29a}$$

$$\widetilde{p}_{\zeta}^{0}(\mu, \zeta_0) = \int_{-\infty}^{+\infty} S_0(\mu, \gamma_0, \zeta_0)\, p_{\gamma}(\gamma_0)\, p_{\zeta}(\zeta_0) \mathrm{d}\gamma_0, \tag{29b}$$

respectively, where the symbol $\widetilde{\ }$ means that shadowing is taken into account.

For the uncorrelated statistical zero-order illumination function, Equation (5) is applied to Equation (29). The integration over ζ_0 does not depend on the height PDF, which leads to:

$$\widetilde{p}^{\,0}_{\gamma,\mathrm{u}}(\mu,\gamma_0)=\frac{\Upsilon(\mu-\gamma_0)}{\Lambda(\mu)+1}p_\gamma(\gamma_0). \tag{30}$$

We assume the slope PDF to be Gaussian, and Equation (29b) becomes:

$$\widetilde{p}^{\,0}_{\zeta,\mathrm{u}}(v,\zeta_0)=\left[1-\frac{1}{2}\mathrm{erfc}(v)\right][F(\zeta_0)]^{\Lambda(v)}p_\zeta(\zeta_0). \tag{31}$$

For a statistical correlated illumination function, Equation (1) is used to replace $S_0(\mu,\gamma_0,\zeta_0)$ in Equation (29). However, it is impossible to simplify because the correlated illumination function S_0 is already obtained by numerical integrations as indicated in Appendix 2. As a result, numerical integrations are performed.

During the calculation, the following variable transformations are performed to reduce the number of variables:

$$s_0=\gamma_0/\left(\sigma_\gamma\sqrt{2}\right),\quad h_0=\zeta_0/\left(\sigma_\zeta\sqrt{2}\right),\quad v=\mu/\left(\sigma_\gamma\sqrt{2}\right). \tag{32}$$

The corresponding Gaussian distributions of normalized slope and height, s_0 and h_0, respectively, become:

$$p_s(s_0)=\frac{1}{\sqrt{\pi}}\exp\left(-s_0^2\right)\quad p_h(h_0)=\frac{1}{\sqrt{\pi}}\exp\left(-h_0^2\right). \tag{33}$$

By doing so, the RMS height σ_ζ and the RMS slope σ_γ are suppressed, which reduces the number of degrees of freedom, and the equations depend only on the deterministic variable v.

Figure 5 compares the zero-order marginal histograms of heights and slopes of the illuminated points, given by the statistical zero-order illumination function with and without correlation and by the Monte Carlo method. The y-scale is changed for each subfigure, so as to show the differences clearly. It is noticeable that the uncorrelated illumination function overestimates the illumination effect as the normalized slope s_0 approaches v, and in the area where the normalized height h_0 is small. But the correlated zero-order marginal histograms overcome these problems and fit the Monte Carlo result very well.

Equation (30) shows that all points with slopes $\gamma_0<\mu$ are shadowed equally. However, this is true only when the correlation between heights and slopes is neglected. It is interesting to have a close look at the angular illumination term of the Smith illumination function, given by:

$$S_\gamma(\mu,\gamma_0)=\int_{-\infty}^{+\infty}S_0(\mu,\gamma_0,\zeta_0)\,p_\zeta(\zeta_0)\mathrm{d}\zeta_0. \tag{34}$$

Neglecting the correlation between heights and slopes in the above equation leads to:

$$S_{\gamma,\mathrm{u}}(\mu,\gamma_0)=\frac{\Upsilon(\mu-\gamma_0)}{\Lambda(\mu)+1}, \tag{35}$$

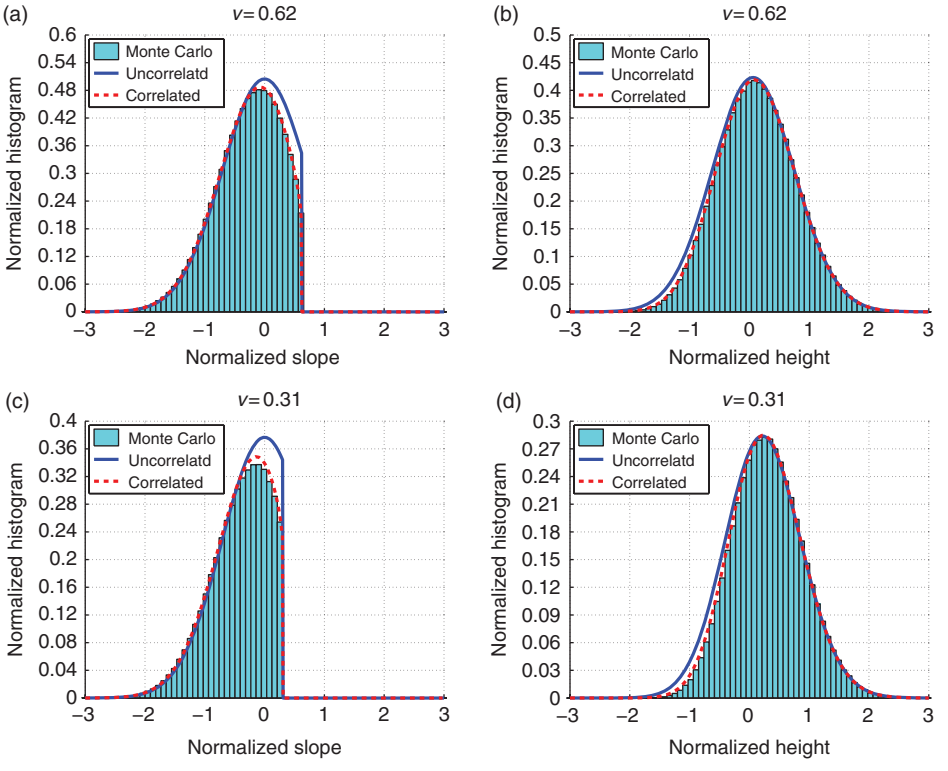

Figure 5. (Color online) Zero-order marginal histogram of slopes (left) and heights (right) versus normalized slope s_0 and height h_0, for $v = 0.62$ (top) and $v = 0.31$ (bottom).

which implies an equal probability of being shadowed for points with slope $\gamma_0 < \mu$. For a correlated illumination function, the result is calculated numerically and plotted in Figure 6. The variable transformations given in Equation (32) are performed during the calculation. It is noticeable that the angular illumination term with correlation bends down as the normalized slope s_0 approaches v, or equally as the slope γ_0 approaches μ. In fact, when Smith [2] deduced the illumination function, he never assumed that all points with slope $\gamma_0 < \mu$ should be equally shadowed. Instead, throughout his deduction, he made two major approximations only: firstly, the probability that 'the ray $M_0(\theta)$ is not shadowed by the sub-surface $l \in (0, \tau)$' is replaced by that 'the ray $M_0(\theta)$ is not shadowed by the point $l = \tau$'. Secondly, the correlation of the heights and slopes is neglected for computational ease. It is shown in Figure 5 that considering the correlation improves the Smith illumination function greatly.

The correlation between two points on the surface is negligible only when the distance of two points $\triangle L$ is larger than the surface correlation length L_c. However, as the height of the emission ray from M_0 at a distance $\triangle L = \tau$ equals $\zeta_0 + \tau\mu$ (see Figure 1), the larger $\triangle L$ is, the higher is the ray at that point, and the weaker

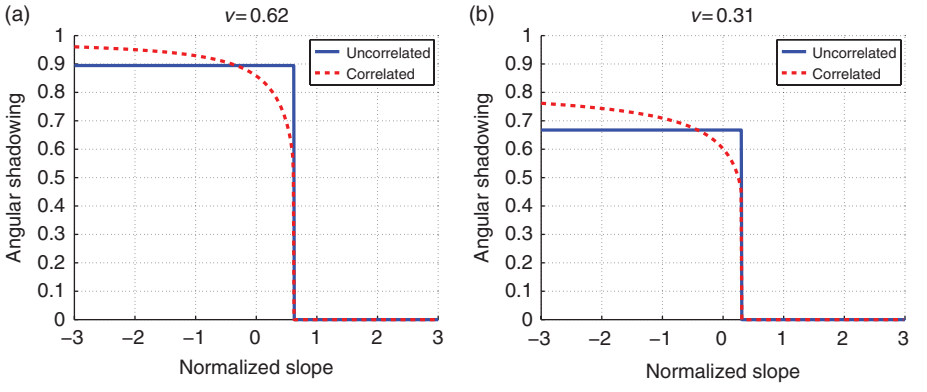

Figure 6. (Color online) Zero-order angular illumination term of the zero-order illumination function with correlation (dashed) and without correlation (solid) versus the normalized slope s_0.

is the probability of having one point on the surface with that height. As a result, given that a ray $M_0(\theta)$ is blocked by the surface, it is more likely that it is blocked by some facet which is close to M_0. In such a case, $\triangle L$ is of the order of the correlation length, which means that the correlation between these points should be considered. Ignoring this correlation leads to the difference between the uncorrelated model and the Monte Carlo result, as shown in Figure 5.

4.2. *Marginal histograms of first-order illumination function*

The first-order marginal histograms of illuminated slopes and heights are defined in a way very similar to that of the zero-order:

$$\begin{aligned}\widetilde{p}^{\,1}_{\gamma}(\mu,\gamma_0) &= \int_{-\infty}^{+\infty} S_1(\mu,\gamma_0,\zeta_0)\,p_\gamma(\gamma_0)\,p_\zeta(\zeta_0)\mathrm{d}\zeta_0\\ \widetilde{p}^{\,1}_{\zeta}(\mu,\zeta_0) &= \int_{-\infty}^{+\infty} S_1(\mu,\gamma_0,\zeta_0)\,p_\gamma(\gamma_0)\,p_\zeta(\zeta_0)\mathrm{d}\gamma_0.\end{aligned} \tag{36}$$

For the uncorrelated first-order illumination function, Equation (24) is applied to Equation (36). For any height PDF, the integration over ζ_0 can be expressed as:

$$\widetilde{p}^{\,1}_{\gamma,\mathrm{u}}(\mu,\gamma_0) = \begin{cases} \dfrac{1}{\Lambda(\mu)+1}p_\gamma(\gamma_0), & \text{cases 1\&4}\\ \dfrac{\Lambda(\mu_1)}{[\Lambda(\mu)+1][\Lambda(\mu_1)+\Lambda(\mu)+1]}\,p_\gamma(\gamma_0), & \text{cases 2\&3}\\ 0, & \text{otherwise.}\end{cases} \tag{37}$$

Unfortunately, as μ_1 is a function of γ_0, the integration over the slope γ_0 must be calculated numerically. Moreover, it depends on the slope PDF, which is assumed

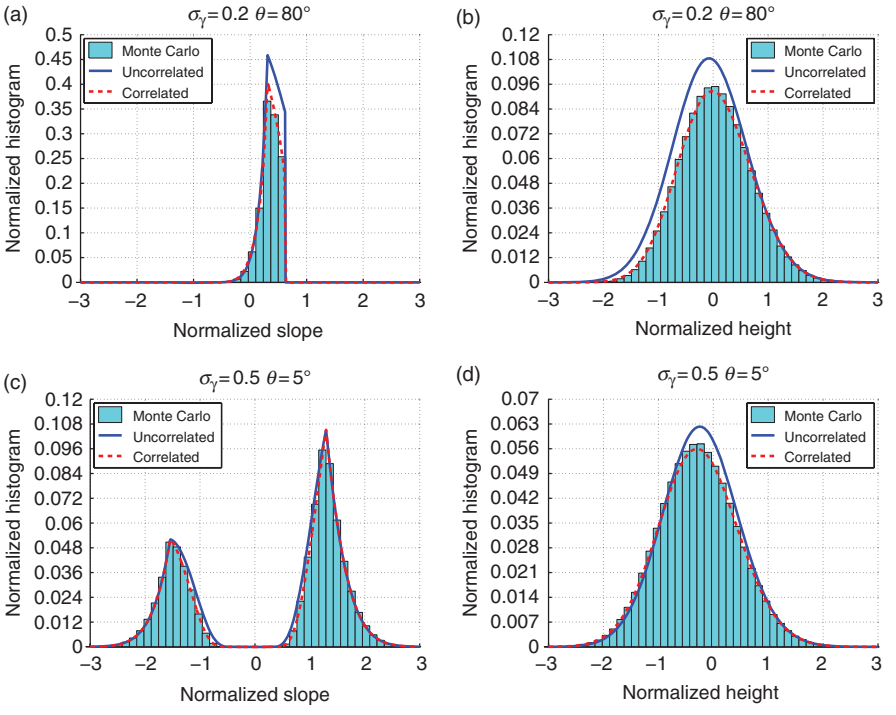

Figure 7. (Color online) First-order marginal histogram of slopes (left) and heights (right) versus the normalized slope s_0 and height h_0 for $\sigma_\gamma = 0.2$, $\theta = 80^\circ$ (top) and $\sigma_\gamma = 0.5$, $\theta = 5^\circ$ (bottom).

to be Gaussian. The marginal histogram of illuminated height is expressed as:

$$\widetilde{p}^{1}_{\zeta,\mathrm{u}}(\mu,\zeta_0) = \left\{ \int_{\gamma_0 \in (\text{cases } 1,4)} p_\gamma(\gamma_0)\mathrm{d}\gamma_0 + \int_{\gamma_0 \in (\text{cases } 2,3)} \left[1 - F(\zeta_0)^{\Lambda(\mu_1)}\right] p_\gamma(\gamma_0)\mathrm{d}\gamma_0 \right\} F(\zeta_0)^{\Lambda(\mu)} p_\zeta(\zeta_0). \quad (38)$$

For a correlated illumination function, Equation (16) is used to replace $S_1(\mu, \gamma_0, \zeta_0)$ in Equation (36) and all the integrations are calculated numerically. The variable transformations given in Equation (32) are also performed during the calculation. However, it is impossible to suppress the dependence on σ_γ here, as θ_1 is a function of θ and γ_0 (see Equation (19)).

The result is shown in Figure 7. The uncorrelated histograms, over the slope and the height of M_0 given by the first-order illumination function, still overestimate the illumination effect. The correlated first-order marginal histograms agree with the Monte Carlo results very well.

4.3. *Average zero- and first-order illumination functions*

In Figure 8, the uncorrelated average zero-order illumination functions is performed for various RMS slopes σ_γ.

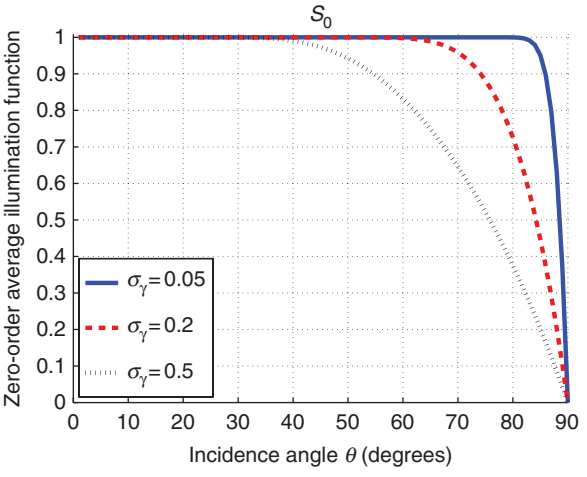

Figure 8. (Color online) Average zero-order illumination function for RMS slope $\sigma_\gamma = 0.05$ (solid), $\sigma_\gamma = 0.2$ (dashed), $\sigma_\gamma = 0.5$ (dotted).

Bourlier et al. showed that for $v > 2$, shadowing is negligible. As a result, the threshold incidence angle of shadowing for a surface with RMS slope σ_γ can be obtained by:

$$\theta_s = \operatorname{arccot}\left(2\sqrt{2}\sigma_\gamma\right). \tag{39}$$

For a surface with small RMS slope, for example $\sigma_\gamma = 0.05$ (solid line in Figure 8), shadowing is very weak. It is shown that even when the observation angle θ is very large, for example $\theta_s \approx 82^\circ$, the average illumination function $S_0 \approx 1$, which means that nearly all the surface is still illuminated. Shadowing is strong only when θ is larger than 82°, with S_0 decreasing rapidly to 0 as θ increases to 90°. Shadowing is more obvious for surfaces with larger RMS slopes. For a surface with $\sigma_\gamma = 0.2$, shadowing occurs when θ is slightly greater than $\theta_s \approx 60^\circ$, and decreases to 0 when $\theta = 90^\circ$ (dashed line in Figure 8). For a surface with $\sigma_\gamma = 0.5$, shadowing is even observed for θ over $\theta_s \approx 35^\circ$ (dotted line in Figure 8).

The average first-order illumination functions, with and without correlation, are plotted in Figure 9 and compared with the Monte Carlo method. As can be predicted by Figure 7, the present model without correlation agrees quite well with the Monte Carlo result. However, it overestimates the illumination effect at large observation angles. With correlation, the result is greatly improved.

It is noticeable that the first-order illumination function is quite large at large observation angles, with a maximum over 0.2, which means that more than 20% of the surface undergoes single surface reflection, at about 75° for a surface with $\sigma_\gamma = 0.2$ and at about 50° for a surface with $\sigma_\gamma = 0.5$. In several papers which deal with surface infrared emissivity [6,7], it is said that the models without considering surface reflections underestimate the surface emissivity in comparison with experiments. As indicated by Bourlier [11], the infrared emissivity of a rough surface

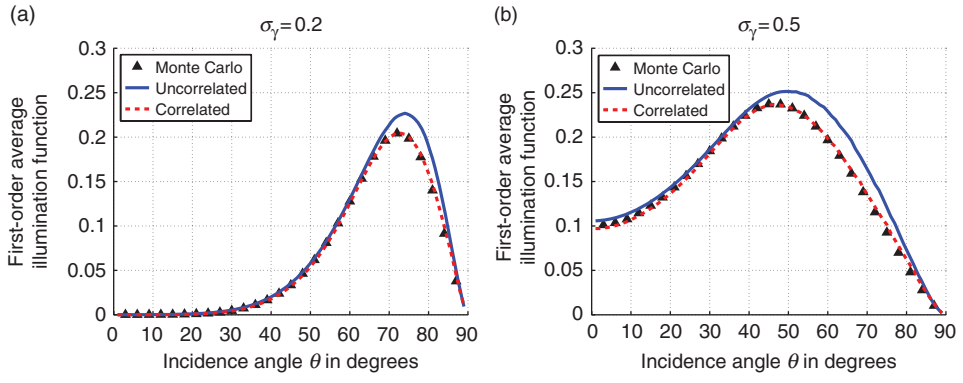

Figure 9. (Color online) Correlated and uncorrelated average first-order illumination function compare with Monte Carlo method for $\sigma_\gamma = 0.2$ (a) and $\sigma_\gamma = 0.5$ (b).

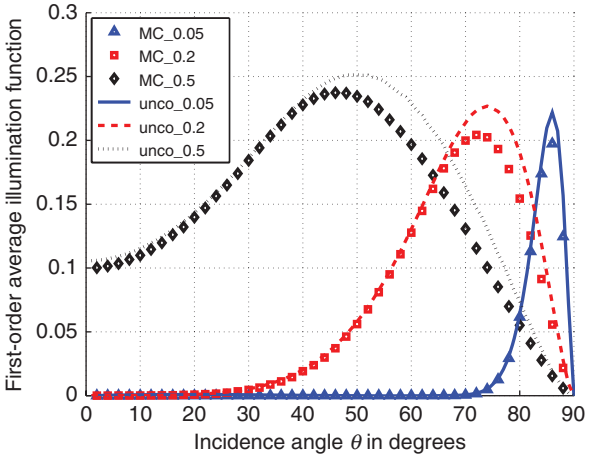

Figure 10. (Color online) Uncorrelated average first-order illumination function for RMS slope $\sigma_\gamma = 0.05$ (solid), $\sigma_\gamma = 0.2$ (dashed), $\sigma_\gamma = 0.5$ (dotted), and the corresponding Monte Carlo results for $\sigma_\gamma = 0.05$ (triangle), $\sigma_\gamma = 0.2$ (square), $\sigma_\gamma = 0.5$ (diamond).

is directly related to the illumination function. Considering the first-order illumination function could be promising to reduce the discrepancy between these infrared emissivity models.

In Figure 10, the uncorrelated average first-order illumination functions are performed for various RMS slopes σ_γ. The corresponding Monte Carlo results are also shown.

For a surface with small RMS slope, for example $\sigma_\gamma = 0.05$ (solid line and triangles in Figure 10), the range of θ where surface reflection happens is small. Moreover, surface reflection happens only in the large observation area,

$\theta \in [75^\circ, 90^\circ]$. A maximum $S_1 \approx 0.23$ is observed at $\theta \approx 85^\circ$, which means that about 23% of the surface has first-order surface reflection when the observation angle is approximately 85°. For a surface with larger RMS slope, for example $\sigma_\gamma = 0.2$ (dashed line and squares in Figure 10), surface reflection is observed in $\theta \in [30^\circ, 90^\circ]$, which is wider and is no longer restricted to large observation angles. A maximum $S_1 \approx 0.23$ is also observed, but at $\theta \approx 75^\circ$. For large observation angles ($\theta \in [85^\circ, 90^\circ]$), only about 0–10% of the surface undergoes surface reflection. For a surface with $\sigma_\gamma = 0.5$ (dotted line and diamonds in Figure 10), surface reflection is widely observed for $\theta \in [0^\circ, 90^\circ]$. It is noticeable that for small observation angles, even for $\theta = 0^\circ$, surface reflection is observed. However, surface reflection is weak in large observation angles, where $S_1 < 0.05$, which means that no more than 5% of the surface can have surface reflection in this area.

In conclusion, zero-order illumination is strong for surfaces with small RMS slopes σ_γ, while first-order illumination is weak. As σ_γ increases, zero-order illumination decreases and first-order illumination increases. For large observation angles $\theta \in [85^\circ, 90^\circ]$, the proportion of illuminated surface is usually small, unless the surface is rather smooth, with $\sigma_\gamma < 0.05$.

5. Empirical approach

The performance of the correlated first-order illumination function is attractive, while the uncorrelated one takes less computation time and meets the practical application requirements better. For example, to compute one single point of the curve of the average first-order illumination function for a surface with $\sigma_\gamma = 0.2$ (Figure 9(a)), the correlated model takes 4.5 s on average, while the uncorrelated model takes 5.5×10^{-4} s only.[5] In this section, we aim at deriving an empirical method to improve the performance of the uncorrelated illumination function.

5.1. *Determination of the empirical factor*

The goal of this subsection is to determine an empirical factor f, which is multiplied by the uncorrelated zero-order illumination function to obtain the empirical zero-order illumination function:

$$S_{0,\mathrm{e}} = f S_{0,\mathrm{u}}. \tag{40}$$

This empirical zero-order illumination function must agree well with the Monte Carlo result. The first-order illumination function, which is based on the zero-order one, would be improved automatically after the zero-order one is corrected.

The first task is to determine the form of the empirical factor. As we discussed in Section 4.1, the drawback of the uncorrelated zero-order shadowing function is that neglecting the correlation between heights and slopes results in an equal probability of illumination for those points with $\gamma < \mu$ (see the solid lines in Figure 6), which leads to the discrepancy shown in Figures 5(a) and 5(c). In fact, the illumination probability should decrease as s approaches v (see the dashed lines in Figure 6). Thus, the empirical factor should generate a curve similar to the angular illumination

factor given by the zero-order illumination function with correlation. We assume that the empirical factor has the following form:

$$f = (B-1)\exp[-C(v-s_0)] + 1 \quad \text{for} \quad s_0 < v, \tag{41}$$

where B and C are constants for any given v. B describes the magnitude of the damping and it ranges from 0 to 1. C controls the rate of convergence. Thus, the empirical factor decreases from 1 to B as s_0 approaches v, which meets our requirement.

The next task is to obtain the parameters B and C. To do so, a series of samples is studied. For a given v, the numerical sample of f is obtained by:

$$f_{\text{num}} = \frac{S_{0,\text{MC}}}{S_{0,\text{u}}}, \tag{42}$$

where $S_{0,\text{MC}}$ is the Monte Carlo result of the zero-order illumination function and $S_{0,\text{u}}$ is the uncorrelated one. B is the fraction given by:

$$B = \frac{S_{0,\text{MC}}(s_0 = v)}{S_{0,\text{u}}(s_0 = v)}. \tag{43}$$

With the least squares method, C can be obtained without difficulty. Substituting B and C back into Equation (46), the empirical factor for a given v is obtained. Taking $v = 0.62$ for example, B and C are given by:

$$B = 0.6030 \quad C = 3.7449. \tag{44}$$

The empirical factor f (dashed line) and the numerical samples f_{num} (scattered points) are shown in Figure 11(a). The least squares method is performed to fit only those points where $f_{\text{num}} < 1$, because $S_{0,\text{MC}}$ and $S_{0,\text{u}}$ are small and more or less the same once $S_{0,\text{MC}}$ exceeds $S_{0,\text{u}}$ (see Figures 5(a) and 5(c)). Multiplying the empirical factor and the angular illumination factor of the uncorrelated zero-order illumination function leads to the zero-order empirical angular illumination factor, which is then compared with that of the zero-order correlated illumination function. It is shown in Figure 11(b) that the empirical angular illumination factor is no longer constant but decreases as s_0 approaches v, which is the same case as in the correlated angular illumination factor. In the region where $f < 1$, the empirical angular illumination factor fits that of the correlated illumination function so well that the empirical illumination function seems to match the performance of the correlated illumination function, which will be examined in the next subsection.

For any v, the previous step is repeated and $B(v)$ and $C(v)$ are obtained. As indicated by Bourlier et al. [3], shadowing can be neglected for $v > 2$. In this paper, all $v \in [0.05, 2]$ are investigated, with a step equal to 0.05. Unfortunately, B and C are not constant but vary with v, as the scattered points shown in Figure 12. As a result, a power 5 polynomial is used to fit the data, which is shown:

$$B = \sum_{i=0}^{i=5} b_i |v|^i, \quad C = \sum_{i=0}^{i=5} c_i |v|^i. \tag{45}$$

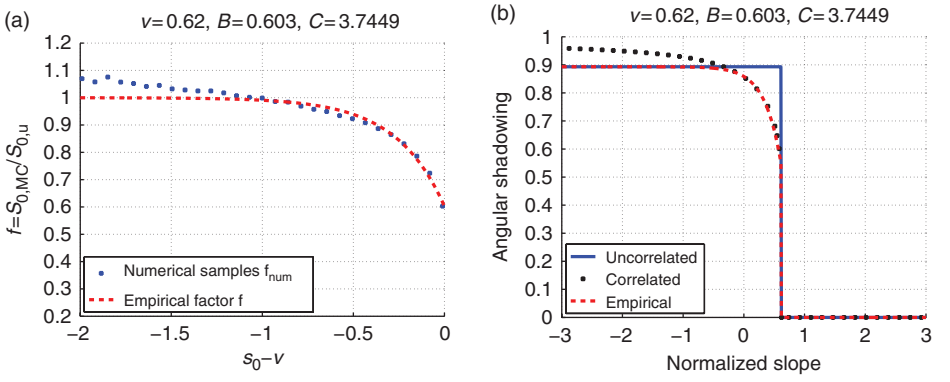

Figure 11. (Color online) Empirical factor together with the numerical samples (a), and the comparison of angular illumination factor of the correlated, uncorrelated and empirical zero-order illumination functions (b).

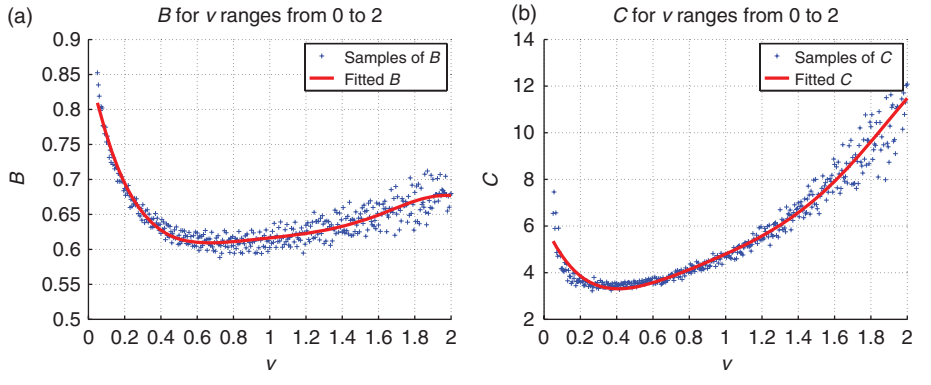

Figure 12. (Color online) B (a) and C (b) for $v \in [0.05, 2]$.

The least squares method is performed again and the parameters b_n and c_n are reported in Table 1. B and C in Equation (45) are shown as solid lines in Figure 12.

Although it is time consuming to obtain all the Monte Carlo results needed to compute b_n and c_n, it is very easy to compute the empirical factor once b_n and c_n are obtained. The data in Table 1 can be used for the region $v \in [0, 2]$, beyond which shadowing is negligible. Thus, the parameters b_n and c_n no longer need to be calculated.

Until now, only the situation where $v > 0$ and $s_0 < v$ is considered. When surface reflections are taken into account, v could be negative and thus s_0 could be larger than v. For $|v| > 2$, shadowing is negligible and the uncorrelated zero-order illumination function would not be very different from the Monte Carlo result, and needs no correction. Thus, f is set to 1 in such regions. The empirical factor

Table 1. Parameters for B and C.

n	0	1	2	3	4	5
b_n	0.8660	1.2388	2.2895	−2.0372	0.8845	−0.1476
c_n	6.1608	−18.0344	39.3244	−36.2345	16.2922	−2.7097

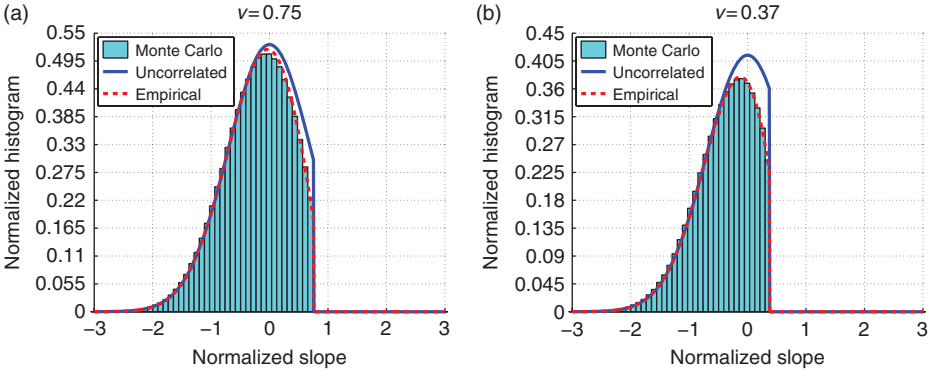

Figure 13. (Color online) Zero-order empirical marginal histogram of illuminated slopes.

is modified as follows to fit all situations:

$$f(v, s_0) = \begin{cases} (B-1)\exp(-C|v-s_0|)+1 & \text{for } v \in [-2, 2] \\ 1 & \text{for otherwise.} \end{cases} \tag{46}$$

5.2. *Simulation of the empirical illumination function*

5.2.1. *Empirical zero-order illumination function*

The zero-order empirical illumination function is obtained by multiplying Equation (5) and Equation (46):

$$S_{0,\mathrm{e}}(\mu, \gamma_0, \zeta_0) = S(\mu, \gamma_0, \zeta_0) \times f. \tag{47}$$

As the empirical factor does not depend on the heights, it does not affect the integration over the height ζ_0. Thus, the zero-order marginal histogram of illuminated slopes is the product of Equations (30) and (46):

$$\widetilde{p}^{\,0}_{\gamma,\mathrm{e}}(\mu, \gamma_0) = \frac{\Upsilon(\mu-\gamma_0)}{\Lambda(\mu)+1} p_\gamma(\gamma_0) \times f. \tag{48}$$

The result is shown in Figure 13. It is shown that the empirical factor improves the performance of the zero-order uncorrelated illumination function.

The average empirical zero-order shadowing function is obtained by averaging Equation (47) over γ_0 and ζ_0. Considering that the sensor is at the right-hand side

of the surface ($v>0$ and $s_0<v$), for a Gaussian slope PDF and with the variable transformations defined in Equation (32), it is given by:

$$\begin{aligned}\overline{\overline{S}}_{0,\mathrm{e}}(v) &= \int_{-\infty}^{+\infty}\int_{-\infty}^{+\infty} S_{0,\mathrm{e}}(\mu,\gamma_0,\zeta_0)\,p_\zeta(\zeta_0)\,p_\gamma(\gamma_0)\mathrm{d}\zeta_0\mathrm{d}\gamma_0 \\ &= \begin{cases} \dfrac{1}{1+\Lambda(v)}\left\{\left[1-\dfrac{1}{2}\mathrm{erfc}(v)\right]+(B-1)\exp\left(-Cv+\dfrac{C^2}{4}\right)\right. & \\ \qquad\left.\times\left[1-\dfrac{1}{2}\mathrm{erfc}\left(v-\dfrac{C}{2}\right)\right]\right\}, & \text{for } v\in[-2,2] \\ \dfrac{1}{1+\Lambda(v)}\left[1-\dfrac{1}{2}\mathrm{erfc}(v)\right], & \text{otherwise.} \end{cases}\end{aligned} \tag{49}$$

5.2.2. *Empirical first-order illumination function*

The first-order empirical illumination function is given by:

$$S_{1,\mathrm{e}}(\mu,\gamma_0,\zeta_0) = \begin{cases} f(v,s_0)F(\zeta_0)^{\Lambda(\mu)}, & \text{cases 1\&4} \\ f(v,s_0)F(\zeta_0)^{\Lambda(\mu)}\left[1-f(v_1,s_0)F(\zeta_0)^{\Lambda(\mu_1)}\right], & \text{cases 2\&3} \\ 0, & \text{otherwise} \end{cases} \tag{50}$$

where $v_1=\mu_1/(\sigma_\gamma\sqrt{2})$. To obtain the average empirical first-order shadowing function, Equation (50) is averaged over γ_0 and ζ_0:

$$\overline{\overline{S}}_{1,\mathrm{e}}(\mu) = \int_{-\infty}^{+\infty}\int_{-\infty}^{+\infty} S_{1,\mathrm{e}}(\mu,\gamma_0,\zeta_0)\,p_\zeta(\zeta_0)\,p_\gamma(\gamma_0)\mathrm{d}\zeta_0\mathrm{d}\gamma_0. \tag{51}$$

The integration over the height ζ_0 can still be done analytically, which is given by:

$$\overline{S}_{1,\mathrm{e}}(\mu,\gamma_0) = \begin{cases} \dfrac{1}{\Lambda(\mu)+1}f(v,s_0), & \text{cases 1\&4} \\ \dfrac{[1-f(v_1,s_0)][\Lambda(\mu)+1]+\Lambda(\mu_1)}{[\Lambda(\mu)+1][\Lambda(\mu_1)+\Lambda(\mu)+1]}f(v,s_0), & \text{cases 2\&3} \\ 0, & \text{otherwise.} \end{cases} \tag{52}$$

Thus, the marginal histogram of illuminated slopes given by the first-order empirical illumination function is expressed analytically by:

$$\widetilde{p}^{1}_{\gamma_0,\mathrm{e}}(\mu,\gamma_0) = \overline{S}_{1,\mathrm{e}}(\mu,\gamma_0)\,p_\gamma(\gamma_0). \tag{53}$$

Results are shown in Figure 14. It can be seen that the empirical illumination function agrees well with the Monte Carlo result at large observation angles (Figure 14(a)). At small observation angles, there is no significant improvement (Figure 14(b)).

As μ_1 and $f(v_1)$ are functions of γ_0, the integration over γ_0 must be performed numerically. The results are shown in Figure 15, where again very good agreements are obtained.

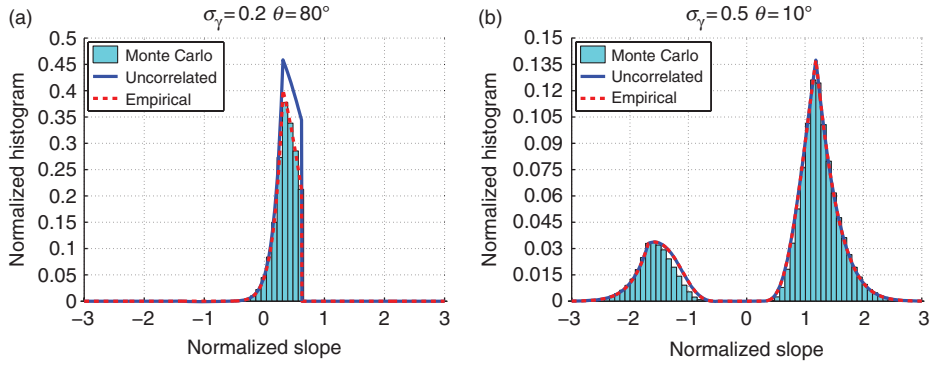

Figure 14. (Color online) First-order empirical marginal histogram of illuminated slopes.

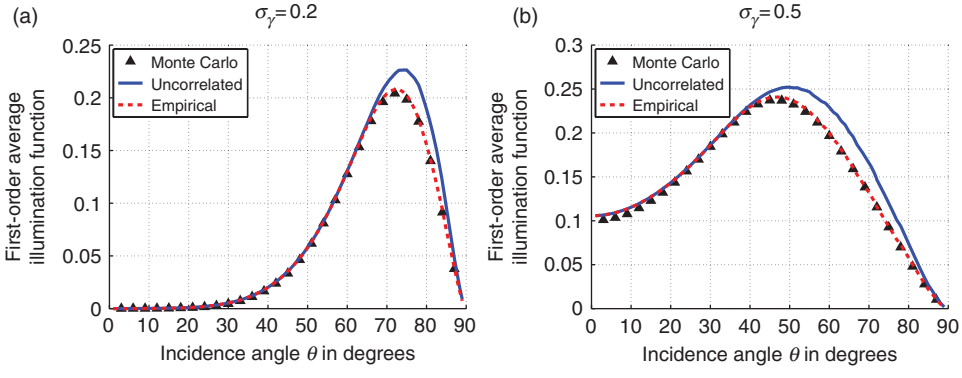

Figure 15. (Color online) Empirical average first-order illumination function compared with the Monte Carlo method for $\sigma_\gamma = 0.2$ (a) and $\sigma_\gamma = 0.5$ (b).

It is shown that the empirical illumination function works quite well, with nearly the same performance as the correlated illumination function. Besides, it consumes much less computation time. Taking the same example as at the beginning of this section: to compute one single point of the curve of the average first-order illumination function for a surface with $\sigma_\gamma = 0.2$, the empirical model takes 1.1×10^{-3} s only. This empirical factor is a good compromise between accuracy and computation time.

6. Conclusion

In this paper, the statistical illumination function with one surface reflection from a one-dimensional random rough surface is developed for a monostatic configuration. The Smith model is used as the basic model, and the first-order illumination is expressed based on the Smith illumination function.

To study the performance of the present model, the PDFs of the surface heights and slopes are assumed to be Gaussian and the average zero-order and first-order illumination functions are computed, for a surface of infinite length. A Monte Carlo ray-tracing algorithm is used as the reference. The contribution of the correlation between heights and slopes is also studied, assuming that the surface height has a Gaussian autocorrelation function. The phenomenon that all slopes are shadowed equally results from neglecting the correlation between heights and slopes of the surface. The first-order illumination function without correlation is satisfactory, although it slightly overestimates the illumination effect at large observation angles. The first-order illumination function with correlation agrees very well with the Monte Carlo result. Then, an empirical factor is introduced for practical purpose. The empirical factor multiplying the uncorrelated illumination function leads to the empirical illumination function, which agrees well with the Monte Carlo method while it consumes little computation time.

The first-order illumination function is very large at large observation angles. It could improve the performance of the existing models of surface emissivity.

Notes

1. Equation (2) holds for rays going right. The function g for rays going left is given in Appendix 5.
2. See Appendix 3 for the calculation of the third threshold value.
3. See Appendix 5 for calculation details.
4. Bourlier et al. denoted the first-order defined here as second-order. M_0 and M_1 are also inversely denoted.
5. For MATLAB running on an office PC, with 3 GHz CPU and 4 GB memory, 32 bit system.

References

[1] R.J. Wagner, *Shadowing of randomly rough surfaces*, J. Opt. Soc. Am. 41 (1967), pp. 138–147.
[2] B.G. Smith, *Geometrical shadowing of a random rough surface*, IEEE Trans. Antennas Propagat. 15 (1967), pp. 668–671.
[3] C. Bourlier, G. Berginc, and J. Saillard, *Monostatic and bistatic shadowing functions from a one-dimensional stationary randomly rough surface according to the observation length: I. Single scattering*, Waves Random Complex Media 12 (2002), pp. 145–173.
[4] L.M. Ricciardi and S. Sato, *A note on first passage time problems for Gaussian processes and varying boundaries*, IEEE Trans. Inf. Theory 29 (1983), pp. 454–457.
[5] L.M. Ricciardi and S. Sato, *On the evaluation of first passage time densities for Gaussian processes*, Signal Process. 11 (1986), pp. 621–627.
[6] X. Wu and W.L. Smith, *Emissivity of rough sea surface for 8–13 μm: modeling and verification*, Appl. Opt. 36 (1997), pp. 2609–2619.
[7] B.G. Henderson, J. Theiler, and P. Villeneuve, *The polarized emissivity of a wind-roughened sea surface: a Monte Carlo model*, Remote Sens. Environ. 88 (2003), pp. 453–467.
[8] K. Masuda, *Infrared sea surface emissivity including multiple reflection effect for isotropic Gaussian slope distribution model*, Remote Sens. Environ. 103 (2006), pp. 488–496.

[9] C. Bourlier, G. Berginc, and J. Saillard, *Monostatic and bistatic shadowing functions from a one-dimensional stationary randomly rough surface: II. Multiple scattering*, Waves Random Complex Media 12 (2002), pp. 175–200.
[10] C. Bourlier, J. Saillard, and G. Berginc, *Intrinsic infrared radiation of the sea surface*, Prog. Electromag. Res. 27 (2000), pp. 185–335.
[11] C. Bourlier, *Unpolarized emissivity with shadow and multiple reflections from random rough surfaces with the geometric optics approximation: application to Gaussian sea surfaces in the infrared band*, Appl. Opt. 45 (2006), pp. 6241–6254.
[12] C. Bourlier, J. Saillard, and G. Berginc, *Effect of correlation between shadowing and shadowed Points on the Wagner and Smith monostatic one-dimensional shadowing functions*, IEEE Trans. Antennas Propagat. 48 (2000), pp. 437–446.

Appendix 1. The derivation of the Smith illumination function

The probability that the ray $M_0(\theta)$ does not cross the surface in the interval $l \in (0, \tau)$ is defined as $S(\mu, \gamma_0, \zeta_0, \tau)$. Then the probability that the ray $M_0(\theta)$ does not cross the surface in the interval $l \in (0, \tau + \triangle\tau)$ equals

$$S(\mu, \gamma_0, \zeta_0, \tau + \triangle\tau) = S(\mu, \gamma_0, \zeta_0, \tau) \cdot [1 - g(\mu|\gamma_0, \zeta_0; \tau)\triangle\tau], \tag{54}$$

where $g(\mu|\gamma_0, \zeta_0; \tau)\triangle\tau$ is the conditional probability that the ray intersects the surface in the range $l \in (\tau, \tau + \triangle\tau)$ given that it does not in the interval $l \in (0, \tau)$ [2].

When $\triangle\tau$ is sufficiently small, Equation (54) results in the following differential equation [2]:

$$\frac{\mathrm{d}S(\mu, \gamma_0, \zeta_0, \tau)}{\mathrm{d}\tau} = -g(\mu|\gamma_0, \zeta_0; \tau) \cdot S(\mu, \gamma_0, \zeta_0, \tau), \tag{55}$$

which can be integrated to yield:

$$S(\mu, \gamma_0, \zeta_0, L_0) = A \cdot \exp\left[-\int_0^{L_0} g(\mu|\gamma_0, \zeta_0; \tau)\mathrm{d}\tau\right], \tag{56}$$

where L_0 is the surface length introduced by Bourlier et al. [3].

To derive the conditional probability, Smith made an approximation which replaces the condition 'the ray $M_0(\theta)$ does not intersect the surface in $l \in (0, \tau)$' with 'the ray $M_0(\theta)$ is not shadowed by the point $l = \tau$', which requires that the surface at $l = \tau$ should be lower than the ray $M_0(\theta)$:

$$\zeta(\tau) < \zeta_0 + \mu\tau, \tag{57}$$

which is symbolically denoted as α. The event 'the ray does intersect the surface in the region $l \in (\tau, \tau + \triangle\tau)$' requires that the surface at $l = \tau$ is lower than the ray $M_0(\theta)$ while at $l = \tau + \triangle\tau$ it is higher than $M_0(\theta)$:

$$\zeta(\tau) < \zeta_0 + \mu\tau \quad \zeta(\tau + \triangle\tau) > \zeta_0 + \mu(\tau + \triangle\tau). \tag{58}$$

As $\triangle\tau$ is small, it is assumed that the surface slope in the interval $l \in (\tau, \tau + \triangle\tau)$ is a constant. According to Equation (58), it is obvious that the slope of the surface in this interval must exceed the slope of the incident ray:

$$\gamma > \mu. \tag{59}$$

Equation (58) together with (59) are symbolically denoted as β. Then, the conditional probability is expressed as:

$$g(\mu|\gamma_0, \zeta_0; \tau)\triangle\tau = p(\beta|\alpha) = \frac{p(\alpha, \beta)}{p(\alpha)}. \tag{60}$$

Suppressing $\triangle\tau$, then $g(\mu|\gamma_0, \zeta_0; \tau)$ is finally given by [2]:

$$g(\mu|\gamma_0, \zeta_0; \tau) = \frac{\int_{\mu}^{+\infty} (\gamma - \mu)\, p(\zeta = \zeta_0 + \mu\tau, \gamma|\zeta_0, \gamma_0; \tau)\mathrm{d}\gamma}{\int_{-\infty}^{+\infty}\int_{-\infty}^{\zeta_0+\mu\tau} p(\zeta, \gamma|\zeta_0, \gamma_0; \tau)\mathrm{d}\gamma\mathrm{d}\zeta}. \tag{61}$$

Appendix 2. Calculation of the correlation

The correlation between heights and slopes in $p(\zeta, \gamma|\zeta_0, \gamma_0; \tau)$ is usually ignored when calculating equation $g(\mu|\gamma_0, \zeta_0; \tau)$. Bourlier et al. studied this correlation and calculated the zero-order illumination function with correlation [3].

For a Gaussian correlated process with four correlated random variables, the conditional probability is given by [10,12]:

$$\begin{aligned} p(\zeta, \gamma|\zeta_0, \gamma_0; \tau) &= \frac{p(\zeta, \gamma, \zeta_0, \gamma_0; \tau)}{p(\zeta_0, \gamma_0)} \\ &= \frac{\sigma_\zeta \sigma_\gamma}{2\pi\sqrt{|[C]|}} \exp\left[-\frac{1}{2}\boldsymbol{V}^T[C]^{-1}\boldsymbol{V} + \frac{\zeta^2}{2\sigma_\zeta^2} + \frac{\zeta^2}{2\sigma_\zeta^2}\right], \end{aligned} \tag{62}$$

where $\boldsymbol{V}$ is the vector containing all the variables

$$\boldsymbol{V}^T = [\zeta, \gamma, \zeta_0, \gamma_0], \tag{63}$$

and $[C]$ is the covariance matrix

$$[C] = \begin{bmatrix} \sigma_\zeta^2 & R_0(\tau) & 0 & R_1(\tau) \\ R_0(\tau) & \sigma_\zeta^2 & -R_1(\tau) & 0 \\ 0 & -R_1(\tau) & \sigma_\gamma^2 & -R_2(\tau) \\ R_1(\tau) & 0 & -R_2(\tau) & \sigma_\gamma^2 \end{bmatrix}, \tag{64}$$

in which $R_0(\tau)$ is the autocorrelation function of the surface height ζ. $R_1(\tau)$ and $R_2(\tau)$ are the first and second derivatives of $R_0(\tau)$, respectively. In this article, $R_0(\tau)$ is chosen as a Gaussian autocorrelation function, given by:

$$R(\tau) = \sigma_\zeta^2 \exp\left(\frac{\tau^2}{L_c^2}\right), \tag{65}$$

where L_c is the surface correlation length.

The function $g_{co}(\mu|\gamma_0, \zeta_0; \tau)$ with correlation is calculated by substituting Equation (62) into (2), after which $g_{co}(\mu|\gamma_0, \zeta_0; \tau)$ is integrated over τ to obtain the illumination function according to Equation (1). Because of the complexity of $g(\mu|\gamma_0, \zeta_0; \tau)$, the integration is performed numerically.

Bourlier et al. indicated that for a Gaussian autocorrelation function, if the horizontal distance τ between two points is larger than three times the correlation length L_c, the correlation can be ignored [12]. As a result, when calculating the correlated illumination function, the integration over τ in the range $\tau \in [0, 3L_c]$ is calculated numerically as explained in the above paragraph, while the integration over $\tau \in [3L_c, +\infty]$ is obtained analytically by:

$$G = \int_{3L_c}^{+\infty} g(\mu|\gamma_0, \zeta_0; \tau)\mathrm{d}\tau = -\ln[F(\zeta_0 + \mu 3L_c)]^{\Lambda(\mu)}. \tag{66}$$

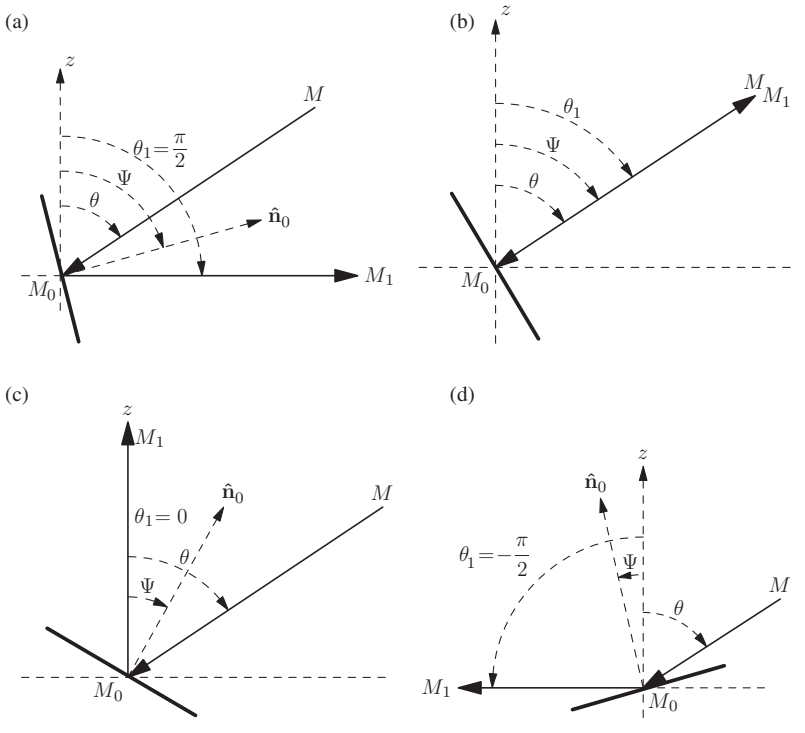

Figure 16. Four threshold values of γ_0.

Finally, the correlated zero-order illumination function is expressed by:

$$S_{\mathrm{co}}(\mu, \gamma_0, \zeta_0) = \Upsilon(\mu - \gamma_0) \times \exp\left[-\int_0^{3L_c} g_{\mathrm{co}}(\mu|\gamma_0.\zeta_0; \tau)\mathrm{d}\tau - G\right]. \tag{67}$$

The correlated first-order illumination function is obtained similarly, with all the integrations of $g(\mu|\gamma_0, \zeta_0; \tau)$ over τ calculated in the same way as shown in Equation (67).

Appendix 3. Identifying four cases by γ_0

To identify the four cases by γ_0, four threshold values of γ_0 should be derived geometrically, shown in Figure 16.

As $\hat{\boldsymbol{n}}_0$ is the angle bisector of $\angle MM_0M_1$, it is always true that:

$$\Psi = \frac{\theta_1 + \theta}{2}. \tag{68}$$

The slope γ_0 can then be expressed as:

$$\gamma_0 = -\tan\Psi = -\tan\left(\frac{\theta_1 + \theta}{2}\right). \tag{69}$$

In Figure 1(a), $\theta_1 = \pi/2$, $\gamma_{\text{th }1} = -\tan(\pi/4 + \theta/2)$. The region $\gamma_0 \in [-\infty, \gamma_{\text{th }1}]$ corresponds to case 1. In Figure 1(b), $\theta_1 = \theta$, $\gamma_{\text{th}2} = -\tan(\theta)$. The region $\gamma_0 \in [\gamma_{\text{th }1}, \gamma_{\text{th}2}]$ corresponds to case 2. As γ_0 increases, the reflected ray enters the region where $0 < \theta_1 < \theta$ and S_1 is defined to be 0. In Figure 1(c), $\theta_1 = 0$, $\gamma_{\text{th}3} = -\tan(\theta/2)$. In Figure 1(d), $\theta_1 = -\pi/2$, $\gamma_{\text{th}4} = -\tan(\theta/2 - \pi/4)$. Between $\gamma_0 = \gamma_{\text{th}3}$ and $\gamma_0 = \gamma_{\text{th}4}$ lies case 3, in which the reflected ray travels leftward and upward. The region $\gamma_0 \in [\gamma_{\text{th}4}, \cot\theta]$ corresponds to case 4. As γ_0 exceeds $\cot\theta$, M_0 is blocked from the sensor by itself and $S_1 = 0$.

Appendix 4. Calculation for case 1

In case 1 ($t_1 = +1$, $q_1 = -1$, $\mu_1 < 0$), M_1 is at the right-hand side of M_0. As a result, $\tau \in [0, +\infty)$. For $t_1 = +1$, $g(\mu_1|\gamma_0, \zeta_0; \tau)$ is expressed exactly as Equation (2). For an infinite surface and for $\mu_1 < 0$, the integration over τ leads to

$$\begin{aligned}\int_0^{+\infty} g(\mu_1|\gamma_0, \zeta_0; \tau)\mathrm{d}\tau &= \mu_1 \Lambda(\mu_1) \int_0^{+\infty} \frac{p_\zeta(\zeta = \zeta_0 + \mu_1\tau)}{F(\zeta = \zeta_0 + \mu_1\tau)}\mathrm{d}\tau \\ &= \Lambda(\mu_1) \int_{\zeta_0}^{-\infty} \frac{p_\zeta(\zeta)}{F(\zeta)}\mathrm{d}\zeta \\ &= \Lambda(\mu_1)\big\{\ln[F(-\infty)] - \ln[F(\zeta_0)]\big\} \\ &= \Lambda(\mu_1)\big\{\ln(0) - \ln[F(\zeta_0)]\big\} \\ &= \Lambda(\mu_1)(-\infty). \end{aligned} \tag{70}$$

From Equation (25), $\Lambda(\mu_1)$ is given here ($t_1 = +1$) by:

$$\Lambda(\mu_1) = \frac{1}{\mu_1} \int_{\mu_1}^{+\infty} (\gamma - \mu_1)\, p_\gamma(\gamma)\mathrm{d}\gamma. \tag{71}$$

As the integration is positive and as μ_1 is negative, $\Lambda(\mu_1)$ is negative. As a result, Equation (70) equals plus infinity.

From Equation (14), $p(b|a)$ is given by

$$p(b|a) = \exp\left[-\int_0^{+\infty} g(\mu_1|\gamma_0, \zeta_0; \tau)\mathrm{d}\tau\right] = \exp(-\infty) = 0. \tag{72}$$

Appendix 5. Calculation for case 3

In case 3 ($t_1 = -1, q_1 = +1, \mu_1 < 0$), M_1 is at the left-hand side of M_0. As a result, $\tau \in (-\infty, 0]$. For $t_1 = -1$, $g(\mu_1|\gamma_0, \zeta_0; \tau)$ is expressed as

$$g(\mu_1|\gamma_0, \zeta_0; \tau) = \frac{\displaystyle\int_{-\infty}^{\mu_1} (\mu_1 - \gamma)\, p(\zeta = \zeta_0 + \mu_1\tau, \gamma|\zeta_0, \gamma_0; \tau)\mathrm{d}\gamma}{\displaystyle\int_{-\infty}^{\infty}\int_{-\infty}^{\zeta_0 + \mu_1\tau} p(\zeta, \gamma|\zeta_0, \gamma_0; \tau)\mathrm{d}\gamma\mathrm{d}\zeta}. \tag{73}$$

From Equation (25), $\Lambda(\mu_1)$ is given here ($t_1 = -1$) by:

$$\Lambda(\mu_1) = \frac{1}{\mu_1} \int_{\mu_1}^{+\infty} (\gamma - \mu_1)\, p_\gamma(\gamma)\mathrm{d}\gamma. \tag{74}$$

The integration over τ leads to

$$\begin{aligned}\int_{-\infty}^{0} g(\mu_1|\gamma_0,\zeta_0;\tau)\mathrm{d}\tau &= -\mu_1\Lambda(\mu_1)\int_{-\infty}^{0}\frac{p_\zeta(\zeta=\zeta_0+\mu_1\tau)}{F(\zeta=\zeta_0+\mu_1\tau)}\mathrm{d}\tau\\ &= -\Lambda(\mu_1)\int_{+\infty}^{\zeta_0}\frac{p_\zeta(\zeta)}{F(\zeta)}\mathrm{d}\zeta\\ &= -\Lambda(\mu_1)\{\ln[F(\zeta_0)]-\ln(1)\}\\ &= -\Lambda(\mu_1)\ln[F(\zeta_0)]. \end{aligned} \tag{75}$$

Thus, from Equation (14), $p(b|a)$ is given by

$$p(b|a)=\exp\left[-\int_{-\infty}^{0} g(\mu_1|\gamma_0,\zeta_0;\tau)\mathrm{d}\tau\right]=F(\zeta_0)^{\Lambda(\mu_1)}. \tag{76}$$